

## Highly Photoconductive InP Quantum Dots Films and Solar Cells

Crisp, Ryan; Kirkwood, Nick; Grimaldi, Gianluca; Kinge, Sachin; Siebbeles, Laurens; Houtepen, Arjan

**DOI**

[10.1021/acsaem.8b01453](https://doi.org/10.1021/acsaem.8b01453)

**Publication date**

2018

**Document Version**

Final published version

**Published in**

ACS Applied Energy Materials

**Citation (APA)**

Crisp, R., Kirkwood, N., Grimaldi, G., Kinge, S., Siebbeles, L., & Houtepen, A. (2018). Highly Photoconductive InP Quantum Dots Films and Solar Cells. *ACS Applied Energy Materials*, 1(11), 6569–6576. <https://doi.org/10.1021/acsaem.8b01453>

**Important note**

To cite this publication, please use the final published version (if applicable). Please check the document version above.

**Copyright**

Other than for strictly personal use, it is not permitted to download, forward or distribute the text or part of it, without the consent of the author(s) and/or copyright holder(s), unless the work is under an open content license such as Creative Commons.

**Takedown policy**

Please contact us and provide details if you believe this document breaches copyrights. We will remove access to the work immediately and investigate your claim.

# Highly Photoconductive InP Quantum Dots Films and Solar Cells

Ryan W. Crisp,<sup>\*,†</sup> Nicholas Kirkwood,<sup>†</sup> Gianluca Grimaldi,<sup>†</sup> Sachin Kinge,<sup>‡</sup> Laurens D. A. Siebbeles,<sup>†</sup> and Arjan J. Houtepen<sup>\*,†</sup>

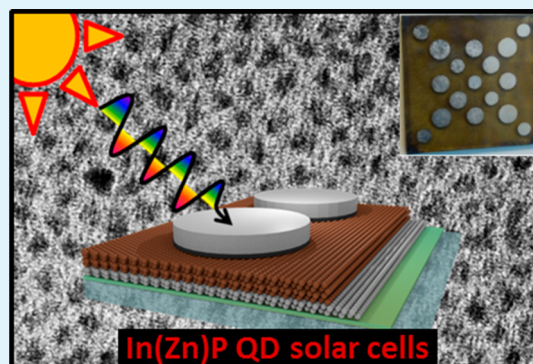
<sup>†</sup>Chemical Engineering Department, Delft University of Technology, Van der Maasweg 9, Delft2629 HZ, The Netherlands

<sup>‡</sup>Toyota Motor Europe, Materials Research & Development, Hoge Wei 33, Zaventem B-1930, Belgium

## Supporting Information

**ABSTRACT:** InP and InZnP colloidal quantum dots (QDs) are promising materials for application in light-emitting devices, transistors, photovoltaics, and photocatalytic cells. In addition to possessing an appropriate bandgap, high absorption coefficient, and high bulk carrier mobilities, the intrinsic toxicity of InP and InZnP is much lower than for competing QDs that contain Cd or Pb—providing a potentially safer commercial product. However, compared to other colloidal QDs, InP QDs remain sparsely used in devices and their electronic transport properties are largely unexplored. Here, we use time-resolved microwave conductivity measurements to study charge transport in films of InP and InZnP colloidal quantum dots capped with a variety of short ligands. We find that transport in InP QDs is dominated by trapping effects, which are mitigated in InZnP QDs. We improve charge carrier mobilities with a range of ligand-exchange treatments and for the best treatments reach mobilities and lifetimes on par with those of PbS QD films used in efficient solar cells. To demonstrate the device-grade quality of these films, we construct solar cells based on InP & InZnP QDs with power conversion efficiencies of 0.65 and 1.2%, respectively. This represents a large step forward in developing Cd- and Pb-free next-generation optoelectronic devices.

**KEYWORDS:** indium phosphide, nanocrystals, quantum dots, photovoltaic, time-resolved microwave conductivity, ligand-exchange



InP and InZnP colloidal quantum dots (QDs) are promising materials as phosphors for lighting and displays, and have been researched for such applications in an effort to replace toxic Cd in CdSe QD displays.<sup>1,2</sup> However, they could also be interesting for LEDs and solar cells given the high absorption coefficient, proper bandgap, and efficient transport properties of bulk InP.<sup>3</sup> There are some papers on InP QD LEDs<sup>4,5</sup> but characterization of charge transport and recombination dynamics within the emissive InP QD films is cursory, limiting the understanding of efficiency loss mechanisms in these devices. There have been a handful of reports using InP QDs in photoconductors<sup>6</sup> and in transistors<sup>7</sup> with few additional reports specifically targeting ligand exchange for improving the transport properties in QD films.<sup>8,9</sup> There are some reports of colloidal InP QDs being used in dye-sensitized solar cells but research into solid-state solar cells is lacking.<sup>10–12</sup>

For QDs, transport of charge carriers depends strongly on the capping ligands that separate the QDs and other surface properties like traps and band positions.<sup>13,14</sup> Understanding and controlling charge transport through these films is critical for optimal performance of devices.<sup>15–17</sup> A high mobility is desired for transistors to have optimal operation as it affects the switching speed and on/off ratios. In prototypical transistors, InP QD films show electron mobilities ranging from  $1 \times 10^{-4} \text{ cm}^2/(\text{V s})$  (with  $\text{In}_2\text{Se}_4^{2-}$  ligands annealed at 250 °C) to  $0.09 \text{ cm}^2/(\text{V s})$  (with  $\text{Sn}_2\text{S}_6^{2-}$  ligands QDs

annealed at 350 °C).<sup>7</sup> These mobilities are orders of magnitude lower than similar CdSe QD transistors.

To better understand the charge carrier dynamics in InP and InZnP QD films, we use time-resolved microwave conductivity (TRMC) to measure the mobility and lifetime of photogenerated charge carriers. TRMC is a contactless spectroscopic technique that can determine the yield of charge carrier generation,  $\phi$ , multiplied by the sum of electron and hole mobility,  $(\mu_e + \mu_h)$ , and the average carrier lifetime,  $\tau$ . With the assumptions that the yield  $\phi$  of photogenerated carriers is near unity, as is commonly found in QD films at room temperature,<sup>18,19</sup> and that within a period of the microwave field the charges probe a volume of material that is representative of the whole system,<sup>20,21</sup> a lower limit on the diffusion length,  $L_D$ , can be calculated. This method is very useful to quickly study materials for solar cells while avoiding troublesome contact optimization.<sup>18,22–25</sup>

Here we make conductive films of InP and InZnP QDs. It has been shown that the addition of Zn to the InP QD synthesis increases the photoluminescence quantum yield (PL QY).<sup>26</sup> There is some discussion in the literature about the atomistic role of the Zn and whether it is on the surface<sup>27</sup> as

**Received:** August 30, 2018

**Accepted:** October 23, 2018

**Published:** October 23, 2018

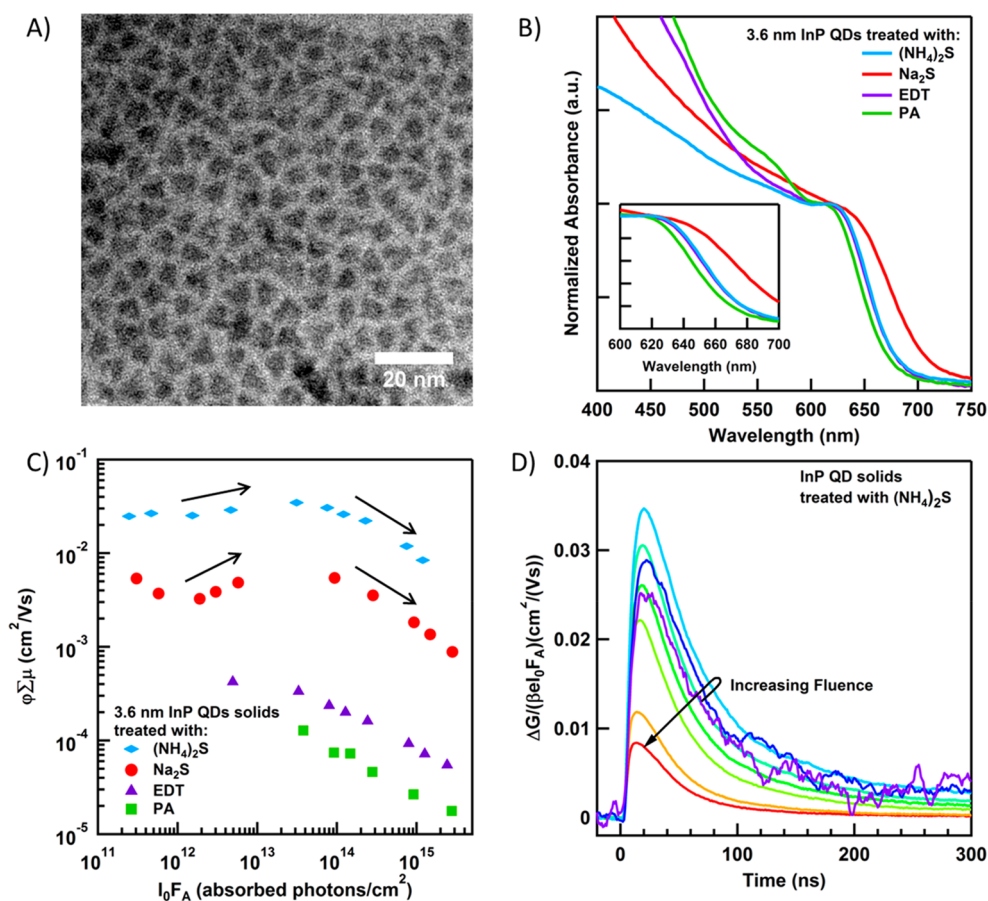


**Figure 1.** (A) TEM image of the PA-capped QDs. (B) Absorption spectra of InP films capped with the ligands noted. EDT = ethanedithiol, PA = palmitate. (C) Fluence-dependence of the sum of the TRMC yield-mobility product for the various QDs capped with the ligands indicated. The leftmost arrows indicate increased trap-filling with increased fluence before the onset of higher-order recombination which again lowers the yield-mobility product (rightmost arrows). (D) Time dependence of the TRMC signal for ammonium sulfide-capped QDs with a half-life of  $\sim 30$  ns.

Zn-carboxylate, in the lattice,<sup>28</sup> or some combination of both.<sup>29</sup> We assess whether it also affects the charge transfer properties of QD films.

## RESULTS AND DISCUSSION

We prepare QD films with a range of surface treatment and show that the TRMC-derived mobility depends strongly on the ligand moiety and Zn content. For the best surface treatments (using  $(\text{NH}_4)_2\text{S}$  or  $\text{Na}_2\text{S}$ ) we reach mobilities of  $\sim 0.04$   $\text{cm}^2/(\text{V s})$  with an average carrier lifetime of up to 60 ns. Comparing the carrier mobility from TRMC measurements of InP QDs to other QD materials indicates that it is lower than sintered Cd-chalcogenide QDs and necked (or epitaxially connected) PbSe QDs ( $\sim 0.1$ – $1$   $\text{cm}^2/(\text{V s})$ )<sup>23,30,31</sup> but is on par with (or higher than) unsintered Cd-chalcogenides and PbS QDs ( $\sim 10^{-3}$ – $10^{-2}$   $\text{cm}^2/(\text{V s})$ ).<sup>19,23,32</sup> We find clear evidence of trap filling in the fluence dependence of the photoconductivity for InP QDs, while this is absent for InZnP QDs. The latter QDs show a clear increase of the mobility with QD size, as expected in a simple random tunneling picture, whereas the mobility in InP QD films shows limited size dependence, perhaps because it is obscured by high trap densities. The lifetime-mobility product obtained with our best treatments is good enough (per ref 33) to produce efficient solar cells. To demonstrate the device-grade quality of these In(Zn)P QD films, we fabricated In(Zn)P solar cells with power conversion efficiencies (PCE) around 1%.

Films of ligand-exchanged InP QDs with or without Zn (hereafter termed In(Zn)P) were fabricated by dipcoating or dropcasting as discussed in the Experimental Methods. Figure 1A shows a TEM micrograph of the starting InP QDs used to determine the QD size along with a sizing curve from Xie et al.<sup>34</sup> (see the Supporting Information for more details). Using these 3.6 nm diameter QDs, the ligands were exchanged from palmitate to ethanedithiol (EDT),  $\text{Na}_2\text{S}$ , or  $(\text{NH}_4)_2\text{S}$ . We note that the last method is a solution-phase ligand exchange; while all other exchanges were performed on QD films.

The absorption spectra of the resulting InP films are shown in Figure 1B and indicate that the QDs retain their quantum confinement, though the first exciton peak shows a red-shift and broadening after the ligand exchange and film-making procedure.<sup>35</sup>

TRMC measurements of the QDs capped with the various ligands (palmitate, ethanedithiol (EDT),  $\text{Na}_2\text{S}$ , and  $(\text{NH}_4)_2\text{S}$ ) are shown in Figure 1C. The yield-mobility product,  $\Phi(t)\sum\mu$ , is plotted versus the absorbed photon fluence for each of the ligands listed. The highest mobility value at lower fluence in the different films spans 2.5 orders of magnitude as the electronic coupling between QDs increases going from palmitate-capped QDs to  $(\text{NH}_4)_2\text{S}$ -treated QDs.<sup>36</sup>  $(\text{NH}_4)_2\text{S}$ -treated QDs have a maximum carrier mobility of  $0.035$   $\text{cm}^2/(\text{V s})$  and a half-life of roughly 30 ns as shown in the TRMC transients in Figure 1D.

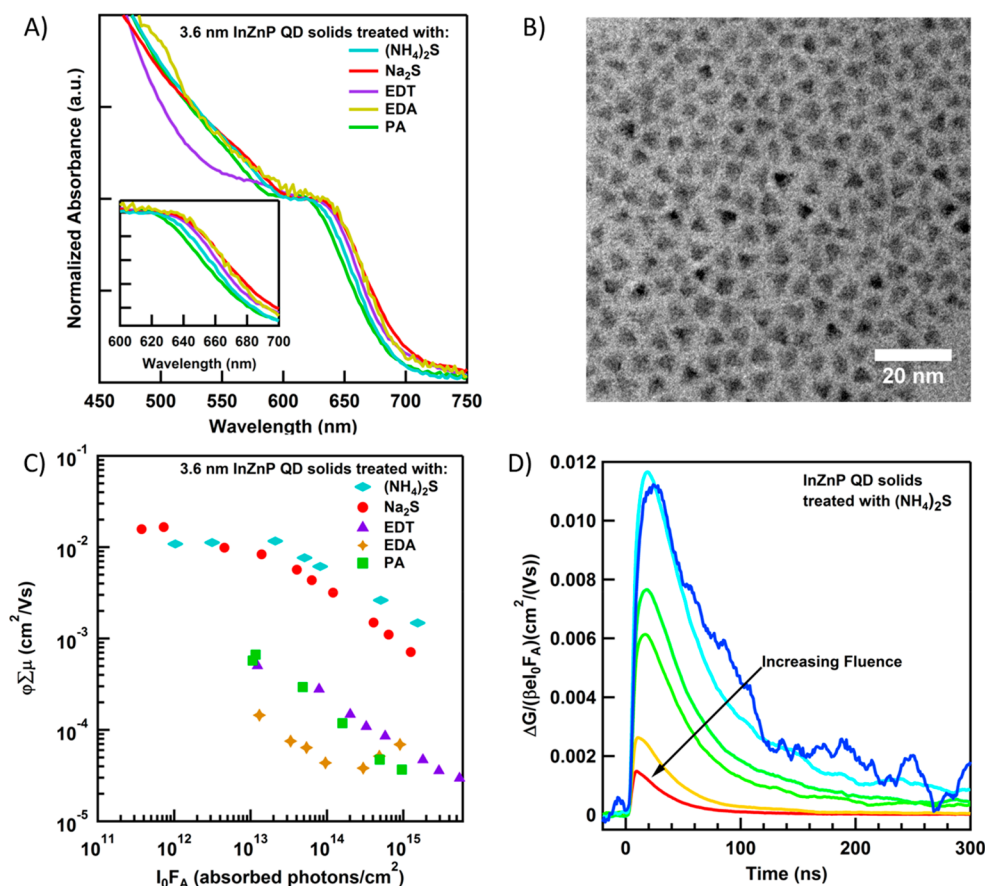


**Figure 2.** (A) Absorption spectra of InZnP films capped with the ligands noted. (B) TEM image of the PA-capped QDs. (C) Fluence-dependence of the sum of the TRMC yield-mobility product for the various QDs capped with the ligands indicated. EDA = ethylenediamine. (D) Time dependence of the TRMC signal for ammonium sulfide-capped QDs with a half-life of 25–60 ns depending on the fluence with lower-fluence having a higher lifetime.

A point of note is that  $\Phi(t) \sum \mu$  initially increases with increasing fluence for Na<sub>2</sub>S and (NH<sub>4</sub>)<sub>2</sub>S ligand treatments, reaching a maximum around 10<sup>14</sup> absorbed photons per cm<sup>2</sup> after which it decreases. If every absorbed photon contributes free carriers with the same mobility, a constant  $\Phi(t) \sum \mu$  is expected.<sup>37,38</sup> The decrease at high fluence is typical for QD films and is attributed higher order decay processes, i.e., Auger recombination.<sup>39</sup>

The increase of  $\Phi(t) \sum \mu$  with increasing fluence is not typically observed in films of Pb- or Cd-chalcogenide QDs, although it has been observed by Savenije et al.<sup>40</sup> for TiO<sub>2</sub> nanoparticles and has been attributed to filling of deep traps. Related, Marino et al.<sup>41</sup> have shown that for CdSe nanoplatelets the PL, surface defects (deep traps), and TRMC mobility are correlated. Such deep traps quickly capture charge carriers within the 3 ns time resolution of the TRMC experiment and hence lower the maximum  $\Phi(t) \sum \mu$  value that is measured.<sup>42</sup> If the lifetime of trapped charges is  $\gg 3$  ns then upon increasing photon fluence traps get filled and the effect of the traps on the photoconductivity per absorbed photon starts to decrease. As shown below, the trap filling effect shows up, to varying extent, for all InP QD sizes and typically saturates around 1 × 10<sup>14</sup> absorbed photons per cm<sup>2</sup>. Combined with a typical film thickness of ~100 nm this corresponds to a very high estimated trap density of 1 × 10<sup>19</sup> cm<sup>-3</sup>.

Similar trends are noted for InZnP QDs with their results summarized in Figure 2. The absorption spectra of the films of ligand exchanged QDs are given in Figure 2A. Here we can see all ligands show a red-shifted absorption onset but interestingly there is no trend in the magnitude of the shift with ligand moiety. A TEM micrograph of the as-synthesized InZnP QDs is shown in Figure 2B and has a similar faceted/trigonal shape as the InP QDs. Figure 2C plots the yield-mobility product as a function of absorbed photon fluence for films of InZnP QDs capped with palmitate ligands (PA) and treated with ethylene diamine (EDA), ethane dithiol (EDT), sodium sulfide (Na<sub>2</sub>S), and ammonium sulfide ((NH<sub>4</sub>)<sub>2</sub>S). The yield-mobility product monotonically decreases with increasing fluence due to higher order recombination events (as discussed above). The time-resolved TRMC signal for the (NH<sub>4</sub>)<sub>2</sub>S-treated InZnP QDs is shown in Figure 2D. At the lowest fluence the half-life time is ~60 ns, roughly double the lifetime of the InP QDs under similar conditions.

Comparing the carrier mobility in InP vs InZnP for a given ligand indicates a factor of 3 lower mobility for InZnP-(NH<sub>4</sub>)<sub>2</sub>S QDs compared to the InP-(NH<sub>4</sub>)<sub>2</sub>S QDs. Furthermore, for InZnP QDs the mobility does not depend on the cation for the S<sup>2-</sup> treatments. With EDT-capping the mobility is the same for both QD types within the error—estimated to be ~20% (see the Supporting Information). Additionally, it is noted that ethylene diamine (EDA) treatment of InZnP QDs yields very similar mobility to the PA-capped QDs indicating

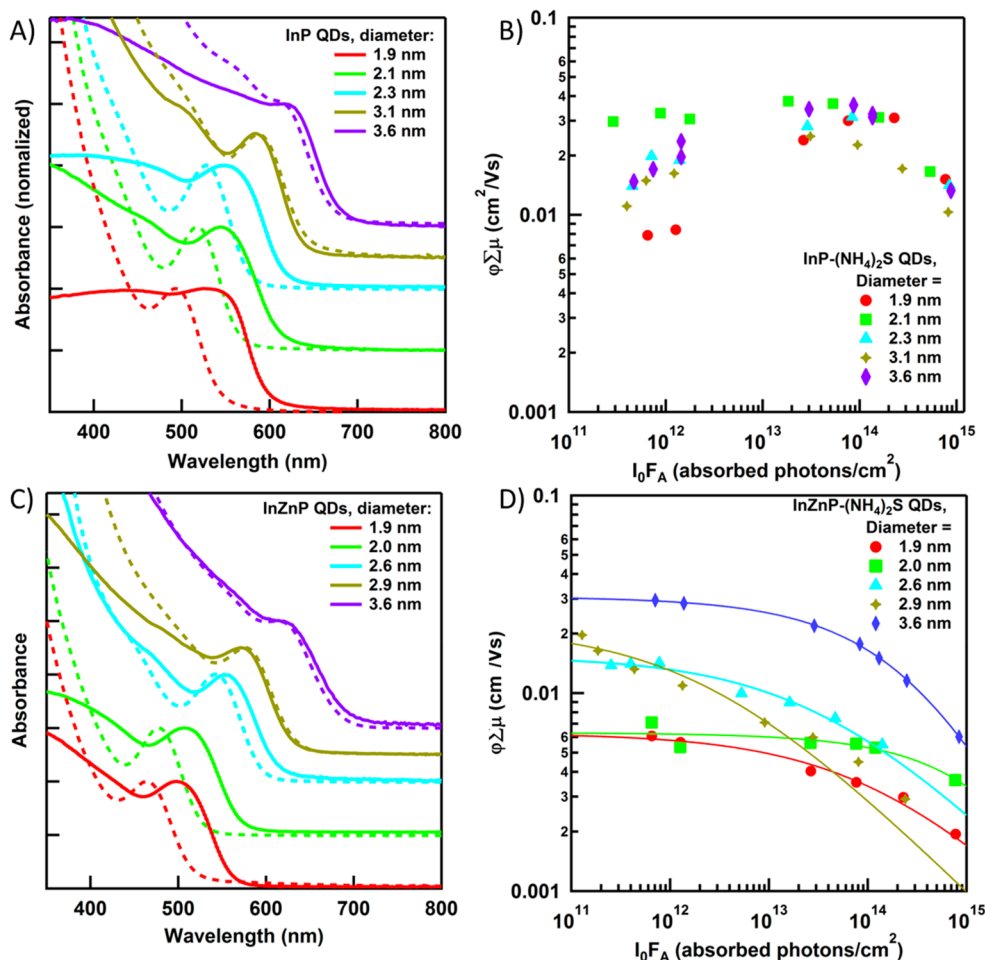


**Figure 3.** (A) Absorption spectra of different sizes of InP QDs capped with  $(\text{NH}_4)_2\text{S}$  both in films (solid lines) and solution (dotted lines), offset for clarity. There are pronounced redshifts from solution to film indicating increased coupling/relaxation of quantum confinement. (B) Fluence-dependence of the TRMC yield-mobility product for InP QDs capped with the ligands indicated and surprisingly showing little variation as a function of size in the peak mobility, with lower mobility at lower fluence indicating a high trap density. (C) Absorption spectra of different sizes of InZnP QDs capped with  $(\text{NH}_4)_2\text{S}$  in films (solid lines) and solution (dotted lines) and offset for clarity. (D) Fluence-dependence of the TRMC yield-mobility product for InZnP QDs showing a clear trend of size with the largest QDs having the highest mobility. Lines are fits to the data as discussed in the text.

these ligand treatments are ineffective at electronically coupling the QDs contrary to the work done on PbSe and CdSe QDs where the mobility improved by orders of magnitude.<sup>31,32,43,44</sup> This is possibly due to the inability of EDA to replace the PA ligands, in line with a slower film build-up than the  $\text{Na}_2\text{S}$  or EDT treatment and the complete absence of build-up for InP QDs further indicating the surface chemistry is different for InP and InZnP. This observation gives some indication that Zn could be on the surface as  $\text{Zn}(\text{PA})_2$  which is potentially more easily removed with EDA than  $\text{In}(\text{PA})_3$ .<sup>27</sup>

Another interesting observation is that for InZnP QDs  $\Phi(t)\sum\mu$  becomes constant at low fluence without any indication of trap filling even for the  $\text{S}^{2-}$  treatments. This suggests that the presence of Zn leads to passivation of the traps that are responsible for the decrease in the photoconductivity in pure InP QDs. This is in line with the higher PL QY of InZnP QDs compared to InP QDs observed in literature and shown in the Supporting Information.<sup>28</sup> Furthermore, varying the Zn/In ratio in the synthesis from 0 to 1 in steps of 0.25 shows lower mobility with increasing Zn but no evidence of trapping in the TRMC signal if Zn is added (see Supporting Information). It seems intuitive that the traps

that are responsible for the decrease in photoconductivity at low fluence and PL could be the same and could be located at the surface. A proper identification of those traps is, however, not permitted by the current experiments.

Next, we explore the size dependence of the QDs using the  $(\text{NH}_4)_2\text{S}$  solution-phase ligand treatment which gives the highest  $\Phi(t)\sum\mu$ . Figure 3 shows the absorption spectra of InP (panel A) and InZnP (panel C) QDs with various sizes both in solution (dotted lines) and after film formation (solid lines) both with  $\text{S}^{2-}$  ligands (exchanged using  $(\text{NH}_4)_2\text{S}$ ) as well as the TRMC results. There are clear spectral shifts to longer wavelengths after film formation, qualitatively indicating increased electronic coupling between the QDs, with a larger red-shift for smaller QDs.

As discussed above, for InP QDs the yield-mobility product in Figure 3B increases with increasing fluence due to trap filling, with a maximum at a fluence of around  $10^{14}$  absorbed photons/ $\text{cm}^2$  then decreases with further increase in fluence due to Auger recombination. The maximum value of  $\Phi(t)\sum\mu$  is plotted in Figure 4 (red circles). As is evident from that figure, there is no clear size dependence of the mobility in

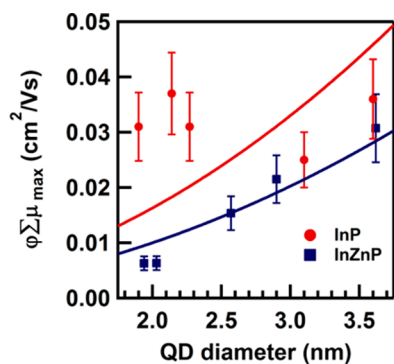


**Figure 4.** Mobility as a function of QD diameter for InP and InZnP showing a size-independent mobility for InP and increasing mobility for increasing QD size for InZnP. The lines are fits using eq 2 (see text).

these InP QD films. Potentially the stronger effect of trap filling obscures size dependence.

Figure 3D shows the fluence dependence of  $\Phi(t)\sum\mu$  for various InZnP QD sizes. Here there is no indication of trap filling and (following refs<sup>45,46</sup>) the data is well-described by the following expression:

$$\Phi_{t=0} \sum \mu = \frac{A}{1 + \sqrt{BI_0 F_A} + CI_0 F_A} \quad (1)$$

This allows us to more reliably extract the low fluence mobility value,  $A$ . The resulting size dependent mobility values are plotted as the blue solid square in Figure 4. For InZnP a clear size dependence of the mobility is observed with larger QDs resulting in higher mobilities.

To understand this size dependent mobility we consider a simple model of charge carriers hopping randomly between nanocrystals with a hopping rate that is independent of QD size (admittedly a strong assumption). In this case, the diffusion of the charge carries will result in a distance  $L$  traveled with time  $t$  that is  $L = \sqrt{6Dt}$  with  $D$  the diffusion coefficient. For a single hop in time,  $\tau_{\text{hop}}$ , this can be written as  $\Delta = \sqrt{6D\tau_{\text{hop}}}$  where  $\Delta$  now represents the center-to-center distance between two QDs. Using the Einstein–Smoluchowski relation this can be expressed as

$$\mu = \frac{\Delta^2 e}{6kT\tau_{\text{hop}}} \quad (2)$$

where  $e$  is the fundamental charge and  $kT$  is the thermal energy. Because  $\Delta = 2R + d$ , where  $R$  is the QD radius and  $d$  is the interparticle spacing, the mobility is expected to increase with  $R$  if the hopping time  $\tau_{\text{hop}}$  is constant. The size dependent mobility is fitted with eq 2 with the result shown as the solid lines in Figure 4. Note that for InP QDs, the fit does not describe the data and makes it clear that there is no size dependence that can be modeled with a simple hopping description. For the InZnP QDs the fit matches the data reasonably well and we extract a hopping time of 35 ps.

The mobility and lifetime measured for these systems are comparable to those of PbS QDs<sup>47</sup> that are used to make quite efficient solar cells. This suggests that it could also be possible to use these In(Zn)P QD films to produce solar cells, with the added benefit of a reduced toxicity. To test if this is indeed the case, we fabricated proof-of-concept solar cells with the largest size of both InP and InZnP QDs following identical film-formation procedures used for TRMC measurements. The device structure is shown in Figure 5 and consists of ITO-coated glass with 40 nm of ZnO as the n-type (or electron accepting) material and MoOx/Ag as the hole contact layers.<sup>48</sup> Resulting  $JV$  curves and solar cell parameters are also shown in Figure 5. For InZnP QDs we achieved an appreciable efficiency of 1.2% while for InP QD solar cells an efficiency of 0.65% was obtained. Differences in the thickness of the cells cause the short circuit current ( $J_{\text{sc}}$ ) to be higher for the InP QD cells as it is  $\sim 180$  nm thick compared to  $\sim 125$  nm for the InZnP QD device, measured using profilometry. We speculate that the larger  $V_{\text{OC}}$  of the InZnP QD cells is due to increased quasi Fermi level splitting between the QDs and the ZnO that is a result of the different trap densities. We stress that these solar cells are clearly not optimized and use, for instance, QDs that are too small to have an optimal bandgap. Further optimization could realistically improve device performance and could represent a path forward to Cd- and Pb-free QD solar cells. On a side note, there are safety concerns about the use of tris(trimethylsilyl)phosphine (P-TMS) as it is pyrophoric; we therefore want to point out efforts toward removing this hazard by using amino phosphine-based precursors for InP QDs in commercial applications.<sup>1,49–53</sup> We also foresee these QDs as potentially useful inks that could then be sintered into bulk thin films, similar to CdTe QDs.<sup>54–56</sup> A more detailed study of the differences in device performance when incorporating Zn into the InP QDs is underway.

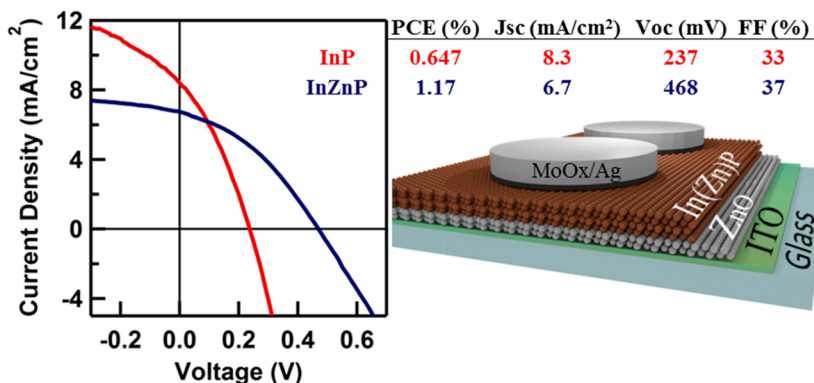


**Figure 5.** Current density–voltage ( $JV$ ) curves for 3.2 nm InP QDs (red) and 2.8 nm InZnP QDs (blue) and the accompanying performance parameters for champion cells with the structure shown in the illustration with an active area of 0.055 cm<sup>2</sup>.

## CONCLUSION

To summarize, charge carrier mobilities and lifetimes for InP and InZnP QDs on par with PbS QDs have been achieved using an  $(\text{NH}_4)_2\text{S}$  solution-phase ligand-exchange procedure. There are strong indications of charge carrier traps and trap filling on a  $\sim 10$  ns time scale in InP QDs that appear to be removed with the inclusion of Zn in the QD synthesis. We observe an increase in mobility with increasing QD size for InZnP, a trend that is obscured by trapping in InP QDs. Utilizing the results, we show proof-of-principle InP and InZnP QD solar cells, achieving PCEs of 0.65 and 1.2%, respectively.

## EXPERIMENTAL METHODS

All chemicals were purchased from Sigma-Aldrich at the highest purity available and used without further modification excluding those described below.

**QD Synthesis.** InP and InZnP QDs were synthesized using stock solutions of indium palmitate ( $\text{In}(\text{PA})_3$ ), zinc palmitate ( $\text{Zn}(\text{PA})_2$ ), and P-TMS. A nitrogen-filled glovebox and standard Schlenk line techniques were followed to keep all reactions air-free. For  $\text{In}(\text{PA})_3$ , 10 mmol of anhydrous indium acetate was added to 40 mmol of palmitic acid in a round-bottom flask. The solution was heated to 140 °C for 6 h. The  $\text{In}(\text{PA})_3$  was precipitated with acetone, filtered and washed again with acetone before being dried under vacuum overnight. The resulting dry powder was then treated with another 40 mmol of palmitic acid (to ensure complete removal of acetate) and washed following the same procedure and stored in a glovebox.

For  $\text{Zn}(\text{PA})_2$ , 2 mmol of sodium palmitate (NaPA) was dissolved in 25 mL methanol in an ultrasonic water bath. 0.18835 g of zinc acetate dissolved in 15 mL methanol was added dropwise with vigorous stirring. A white precipitate of zinc palmitate immediately formed. After 1 h of stirring, the white precipitate was isolated by vacuum filtration, washed three times with methanol, and dried under a vacuum overnight before being stored in a glovebox.

From these stock solutions, 106 mg of  $\text{In}(\text{PA})_3$  (0.12 mmol) and 69 mg  $\text{Zn}(\text{PA})_2$  (0.12 mmol) for InZnP QDs were mixed together with 7 mL of 1-octadecene (ODE) in a three-neck flask, degassed under vacuum for 30 min at 100 °C, and flushed with nitrogen on a Schlenk line. The reaction mixture was heated to 300 °C under nitrogen flow and 17  $\mu\text{L}$  of P-TMS (0.06 mmol) in 1 mL of ODE was rapidly injected. The temperature was lowered to 270 °C and held here for 5 min. After this time, the particles were grown with additional precursors to the desired size. For the growth solution, 441 mg indium palmitate (0.5 mmol) and, additionally for InZnP QDs, 288 mg of zinc palmitate (0.5 mmol) were dissolved in 5 mL of ODE. Separately, 73  $\mu\text{L}$  of P-TMS (0.25 mmol) was dissolved in 3 mL of ODE and loaded into a syringe. 1.67 mL of the In (and Zn) growth solution was injected into the solution, after which the P-TMS growth solution was added over 3 h at a rate of 1 mL/hour using a syringe pump. Every hour, another 1.67 mL of the In (and Zn) growth solution was added. When the desired size was reached, the QDs were cooled to 50 °C and 8 mL of toluene was added. The QDs were washed three times under inert atmosphere via precipitation with methyl acetate, centrifuged at 3800 rpm (1800 rcf), and dispersed in toluene. After the final wash, the QDs were dispersed in hexane for dip coating.

**Ligand Exchange and Film Formation.** The native palmitate ligands will result in an electrically insulating film and, therefore, need to be replaced by shorter or more conductive ones for device applications. Ligand exchange and film formation were carried out by layer-by-layer deposition using a mechanical dipcoater (Nima DC Multi 5.3) in a nitrogen-filled glovebox. The quartz substrate was dipped into In(Zn)P quantum dots dispersed in 2.5 mL of hexane for 5 s. Subsequently, it was dipped into a 0.1 M solution in methanol for 120 s (for  $\text{Na}_2\text{S}$  and EDA) or 30 s (EDT), and rinsed in acetonitrile for 20 s. The dipping speed was 100 mm/min, except when the substrate was raised from the sodium sulfide ( $\text{Na}_2\text{S}$ ) ligand solution, it moved at 200 mm/min, and when lowered into the acetonitrile

solution it moved at 500 mm/min. These faster rates are required for the rinsing process, as acetonitrile can only wash off excess  $\text{Na}_2\text{S}$  before the methanol evaporates. The ammonium sulfide ( $(\text{NH}_4)_2\text{S}$ ) ligand exchange was carried out by phase transfer from hexane to formamide by adding 100  $\mu\text{L}$  of 0.1 M  $(\text{NH}_4)_2\text{S}$  in formamide to bottom 1.5 mL of formamide and stirring vigorously until complete phase exchange from the top hexane phase occurred.<sup>57,58</sup> The solution was rinsed 3 times with hexane, precipitated with acetonitrile and centrifugation at 1800 rcf, and redispersed in *N,N*-dimethylformamide (DMF). Films of QDs exchanged with  $(\text{NH}_4)_2\text{S}$  were dropcast from DMF onto quartz substrates on a hot plate at 50 °C. Ligand exchange with metal halides was also attempted but did not result in high-quality QD films (see the Supporting Information).

**Time-Resolved Microwave Conductivity (TRMC).** TRMC measures the photoconductivity of a sample using microwaves after charge carriers are generated with a laser pulse. To briefly describe the setup, we placed a film of nanocrystals in a microwave waveguide and illuminated them with a pulsed nanosecond laser that has a tunable wavelength in order to excite carriers in the films with different energies. Simultaneously, microwaves are incident on the sample. Whenever free charge carriers are created, they absorb microwaves and we measure a change in the microwave power. Using  $\frac{\Delta P}{P} = -K\Delta G(t)$  we can find the change in photoconductance ( $\Delta G$ ) as a function of time.  $\Delta G$  is then related to the yield ( $\Phi$ ) and the sum of the electron and hole mobility ( $\mu$ ) by  $\Delta G(t) = e\beta I_0 F_a \Phi(t) \sum \mu$  where  $e$  is the electronic charge,  $\beta$  is a ratio of the dimensions of the waveguide, and  $I_0 F_a$  is the absorbed laser fluence of the sample. The yield is the fraction of free charges produced per photon absorbed. Assuming unity yield, the yield-mobility products shown here represent a lower bound to the mobility and could be higher if exciton dissociation is not complete. Using the equations above we can then calculate how the yield-mobility product changes with the various materials and treatments.<sup>38,59</sup>

**UV-Vis Absorption.** Absorption measurements were performed on either a PerkinElmer Lambda 40 or Lambda 1050 (equipped with an integrating sphere for film measurements).

**Transmission Electron Microscopy (TEM).** TEM was performed with a JEOL-JEM 3200 FSC microscope operating at 300 kV. The sizes of the nanocrystals were determined using the first exciton absorption peak in conjunction with a sizing curve as discussed in the Supporting Information (see Supporting Note 1) and verified to be within 10% deviation for the largest sizes with the TEM micrographs shown.

Profilometry, film thicknesses are found by scratching the film to make a step and measuring the step-height using a Dektak profilometer.

**Device Fabrication.** ZnO sol-gel was made by adding 8 mL of 2-methoxyethanol (MEA) (anhydrous) and subsequently 0.2 mL monoethanolamine (EA) (anhydrous) to 800 mg zinc acetate dihydrate in a 10 mL of vial and stirred overnight following modified literature procedures.<sup>22,60,61</sup> The ZnO was spin coated onto ITO-coated glass substrates (MTI Corp, 7–10 Ohms/sq, 180 nm thick) in the fume hood. 70  $\mu\text{L}$  of ZnO was pipetted into the center of the substrate completely filling it. After spinning at 3000 rpm for 45 s, the substrate was annealed on the hot plate in air for 5 min at 260 °C. InP- $(\text{NH}_4)_2\text{S}$  and InZnP- $(\text{NH}_4)_2\text{S}$  were deposited by drop-casting from DMF as described in the film formation section above. Thermal evaporation through a shadow mask of 10 nm of  $\text{MoO}_3$  and 200 nm of Ag with active areas of 0.055, 0.087, and 0.11  $\text{cm}^2$  completes the devices in a similar architecture reported for PbS QD solar cells.<sup>48</sup> Device performance was measured using an OAI TriSol class AAA solar simulator and Keithley 2604 source-measure unit in both the forward and reverse sweeps and show minimal hysteresis.

## ASSOCIATED CONTENT

### Supporting Information

The Supporting Information is available free of charge on the ACS Publications website at DOI: 10.1021/acsam.8b01453.

Reproducibility studies, photoluminescence spectra, additional QD size, ligand, and Zn-content dependence on the mobility, sizing curve discussion, and attempts at ligand exchange with metal halides (PDF)

## AUTHOR INFORMATION

### Corresponding Authors

\*Email: [R.W.Crisp@TUDelft.nl](mailto:R.W.Crisp@TUDelft.nl).

\*Email: [A.J.Houtepen@TUDelft.nl](mailto:A.J.Houtepen@TUDelft.nl). Website: [www.tudelft.nl/cheme/houtepengroup](http://www.tudelft.nl/cheme/houtepengroup).

### ORCID

Ryan W. Crisp: 0000-0002-3703-9617

Nicholas Kirkwood: 0000-0002-7845-7081

Laurens D. A. Siebbeles: 0000-0002-4812-7495

Arjan J. Houtepen: 0000-0001-8328-443X

### Author Contributions

The manuscript was written through contributions of all authors. All authors have given approval to the final version of the manuscript.

### Notes

The authors declare no competing financial interest.

## ACKNOWLEDGMENTS

R.W.C., G.G., S.K., L.D.A.S., and A.J.H. were supported by STW (project 13903, Stable and Non-Toxic Nanocrystal Solar Cells). A.J.H. and N.K. further acknowledge support from the European Research Council Horizon 2020 ERC Grant Agreement 678004 (Doping on Demand).

## REFERENCES

- Reiss, P.; Carrière, M.; Lincheneau, C.; Vaure, L.; Tamang, S. Synthesis of Semiconductor Nanocrystals, Focusing on Nontoxic and Earth-Abundant Materials. *Chem. Rev.* **2016**, *116* (18), 10731–10819.
- Cossairt, B. M. Shining Light on Indium Phosphide Quantum Dots: Understanding the Interplay among Precursor Conversion, Nucleation, and Growth. *Chem. Mater.* **2016**, *28* (20), 7181–7189.
- Bachmann, K. Properties, preparation, and device applications of indium phosphide. *Annu. Rev. Mater. Sci.* **1981**, *11* (1), 441–484.
- Yang, X.; Zhao, D.; Leck, K. S.; Tan, S. T.; Tang, Y. X.; Zhao, J.; Demir, H. V.; Sun, X. W. Full Visible Range Covering InP/ZnS Nanocrystals with High Photometric Performance and Their Application to White Quantum Dot Light-Emitting Diodes. *Adv. Mater.* **2012**, *24* (30), 4180–4185.
- Lim, J.; Park, M.; Bae, W. K.; Lee, D.; Lee, S.; Lee, C.; Char, K. Highly Efficient Cadmium-Free Quantum Dot Light-Emitting Diodes Enabled by the Direct Formation of Excitons within InP@ZnSe Quantum Dots. *ACS Nano* **2013**, *7* (10), 9019–9026.
- Biebersdorf, A.; Dietmüller, R.; Susa, A. S.; Rogach, A. L.; Poznyak, S. K.; Talapin, D. V.; Weller, H.; Klar, T. A.; Feldmann, J. Semiconductor Nanocrystals Photosensitize C60 Crystals. *Nano Lett.* **2006**, *6* (7), 1559–1563.
- Liu, W.; Lee, J.-S.; Talapin, D. V. III-V Nanocrystals Capped with Molecular Metal Chalcogenide Ligands: High Electron Mobility and Ambipolar Photoresponse. *J. Am. Chem. Soc.* **2013**, *135* (4), 1349–1357.
- Dirin, D. N.; Dreyfuss, S.; Bodnarchuk, M. I.; Nedelcu, G.; Papagiorgis, P.; Itskos, G.; Kovalenko, M. V. Lead Halide Perovskites and Other Metal Halide Complexes As Inorganic Capping Ligands for Colloidal Nanocrystals. *J. Am. Chem. Soc.* **2014**, *136* (18), 6550–6553.
- Beard, M. C.; Turner, G. M.; Murphy, J. E.; Micic, O. I.; Hanna, M. C.; Nozik, A. J.; Schmuttenmaer, C. A. Electronic Coupling in InP Nanoparticle Arrays. *Nano Lett.* **2003**, *3* (12), 1695–1699.
- Zaban, A.; Mičić, O. I.; Gregg, B. A.; Nozik, A. J. Photosensitization of Nanoporous TiO<sub>2</sub> Electrodes with InP Quantum Dots. *Langmuir* **1998**, *14* (12), 3153–3156.
- Yang, S.; Zhao, P.; Zhao, X.; Qu, L.; Lai, X. InP and Sn:InP based quantum dot sensitized solar cells. *J. Mater. Chem. A* **2015**, *3* (43), 21922–21929.
- Jamshidi Zavaraki, A.; Huang, J.; Ji, Y.; Ågren, H. Low toxic Cu<sub>2</sub>GeS<sub>3</sub>/InP quantum dot sensitized infrared solar cells. *J. Renewable Sustainable Energy* **2018**, *10* (4), 043710.
- Talapin, D. V.; Lee, J.-S.; Kovalenko, M. V.; Shevchenko, E. V. Prospects of colloidal nanocrystals for electronic and optoelectronic applications. *Chem. Rev.* **2010**, *110* (1), 389–458.
- Hoffman, J. B.; Alam, R.; Kamat, P. V. Why Surface Chemistry Matters for QD–QD Resonance Energy Transfer. *ACS Energy Letters* **2017**, *2* (2), 391–396.
- Kholmicheva, N.; Moroz, P.; Eckard, H.; Jensen, G.; Zamkov, M. Energy Transfer in Quantum Dot Solids. *ACS Energy Letters* **2017**, *2*, 154–160.
- Park, J. H.; Kim, D. Y.; Schubert, E. F.; Cho, J.; Kim, J. K. Fundamental Limitations of Wide-Bandgap Semiconductors for Light-Emitting Diodes. *ACS Energy Letters* **2018**, *3*, 655–662.
- Wang, R.; Shang, Y.; Kanjanaboos, P.; Zhou, W.; Ning, Z.; Sargent, E. H. Colloidal quantum dot ligand engineering for high performance solar cells. *Energy Environ. Sci.* **2016**, *9* (4), 1130–1143.
- Talgorn, E.; Gao, Y.; Aerts, M.; Kunneman, L. T.; Schins, J. M.; Savenije, T. J.; van Huis, M. A.; van der Zant, H. S. J.; Houtepen, A. J.; Siebbeles, L. D. A. Unity quantum yield of photogenerated charges and band-like transport in quantum-dot solids. *Nat. Nanotechnol.* **2011**, *6* (11), 733–739.
- Zhao, T.; Goodwin, E. D.; Guo, J.; Wang, H.; Diroll, B. T.; Murray, C. B.; Kagan, C. R. Advanced Architecture for Colloidal PbS Quantum Dot Solar Cells Exploiting a CdSe Quantum Dot Buffer Layer. *ACS Nano* **2016**, *10* (10), 9267–9273.
- Gao, Y.; Talgorn, E.; Aerts, M.; Trinh, M. T.; Schins, J. M.; Houtepen, A. J.; Siebbeles, L. D. A. Enhanced Hot-Carrier Cooling and Ultrafast Spectral Diffusion in Strongly Coupled PbSe Quantum-Dot Solids. *Nano Lett.* **2011**, *11* (12), 5471–5476.
- Lanzani, G. *Photophysics of Molecular Materials: From Single Molecules to Single Crystals*; John Wiley & Sons: 2006.
- Crisp, R. W.; Panthani, M. G.; Rance, W. L.; Duenow, J. N.; Parilla, P. A.; Callahan, R.; Dabney, M. S.; Berry, J. J.; Talapin, D. V.; Luther, J. M. Nanocrystal Grain Growth and Device Architectures for High-Efficiency CdTe Ink-Based Photovoltaics. *ACS Nano* **2014**, *8* (9), 9063–9072.
- Crisp, R. W.; Callahan, R.; Reid, O. G.; Dolzhenkov, D. S.; Talapin, D. V.; Rumbles, G.; Luther, J. M.; Kopidakis, N. Photoconductivity of CdTe Nanocrystal-Based Thin Films: Te(2–) Ligands Lead To Charge Carrier Diffusion Lengths Over 2 μm. *J. Phys. Chem. Lett.* **2015**, *6* (23), 4815–4821.
- Kroeze, J. E.; Savenije, T. J.; Vermeulen, M. J. W.; Warman, J. M. Contactless Determination of the Photoconductivity Action Spectrum, Exciton Diffusion Length, and Charge Separation Efficiency in Polythiophene-Sensitized TiO<sub>2</sub> Bilayers. *J. Phys. Chem. B* **2003**, *107* (31), 7696–7705.
- Ghosh, T.; Gopal, A.; Nagasawa, S.; Mohan, N.; Saeki, A.; Nair, V. C. Following the TRMC Trail: Optimization of Photovoltaic Efficiency and Structure–Property Correlation of Thiophene Oligomers. *ACS Appl. Mater. Interfaces* **2016**, *8* (38), 25396–25404.
- Xu, S.; Ziegler, J.; Nann, T. Rapid synthesis of highly luminescent InP and InP/ZnS nanocrystals. *J. Mater. Chem.* **2008**, *18* (23), 2653–2656.
- Stein, J. L.; Mader, E. A.; Cossairt, B. M. Luminescent InP Quantum Dots with Tunable Emission by Post-Synthetic Modification with Lewis Acids. *J. Phys. Chem. Lett.* **2016**, *7* (7), 1315–1320.
- Pietra, F.; De Trizio, L.; Hoekstra, A. W.; Renaud, N.; Prato, M.; Grozema, F. C.; Baesjou, P. J.; Koole, R.; Manna, L.; Houtepen, A. J. Tuning the Lattice Parameter of In<sub>x</sub>Zn<sub>y</sub>P for Highly Luminescent Lattice-Matched Core/Shell Quantum Dots. *ACS Nano* **2016**, *10* (4), 4754–62.

- (29) Huang, K.; Demadrille, R.; Silly, M. G.; Sirotti, F.; Reiss, P.; Renault, O. Internal Structure of InP/ZnS Nanocrystals Unraveled by High-Resolution Soft X-ray Photoelectron Spectroscopy. *ACS Nano* **2010**, *4* (8), 4799–4805.
- (30) Talgorn, E.; Abellon, R. D.; Kooyman, P. J.; Piris, J.; Savenije, T. J.; Goossens, A.; Houtepen, A. J.; Siebbeles, L. D. A. Supercrystals of CdSe Quantum Dots with High Charge Mobility and Efficient Electron Transfer to TiO<sub>2</sub>. *ACS Nano* **2010**, *4* (3), 1723–1731.
- (31) Gao, Y.; Aerts, M.; Sandeep, C. S. S.; Talgorn, E.; Savenije, T. J.; Kinge, S.; Siebbeles, L. D. A.; Houtepen, A. J. Photoconductivity of PbSe Quantum-Dot Solids: Dependence on Ligand Anchor Group and Length. *ACS Nano* **2012**, *6* (11), 9606–9614.
- (32) Talgorn, E.; Moysidou, E.; Abellon, R. D.; Savenije, T. J.; Goossens, A.; Houtepen, A. J.; Siebbeles, L. D. A. Highly Photoconductive CdSe Quantum-Dot Films: Influence of Capping Molecules and Film Preparation Procedure. *J. Phys. Chem. C* **2010**, *114* (8), 3441–3447.
- (33) Guyot-Sionnest, P. Electrical Transport in Colloidal Quantum Dot Films. *J. Phys. Chem. Lett.* **2012**, *3* (9), 1169–1175.
- (34) Xie, R.; Li, Z.; Peng, X. Nucleation Kinetics vs Chemical Kinetics in the Initial Formation of Semiconductor Nanocrystals. *J. Am. Chem. Soc.* **2009**, *131* (42), 15457–15466.
- (35) Sandeep, C. S. S.; Cate, S. t.; Schins, J. M.; Savenije, T. J.; Liu, Y.; Law, M.; Kinge, S.; Houtepen, A. J.; Siebbeles, L. D. A. High charge-carrier mobility enables exploitation of carrier multiplication in quantum-dot films. *Nat. Commun.* **2013**, *4*, 2360.
- (36) Crisp, R. W.; Schrauben, J. N.; Beard, M. C.; Luther, J. M.; Johnson, J. C. Coherent Exciton Delocalization in Strongly Coupled Quantum Dot Arrays. *Nano Lett.* **2013**, *13* (10), 4862–4869.
- (37) Martin, S. T.; Herrmann, H.; Hoffmann, M. R. Time-resolved microwave conductivity. Part 2.-Quantum-sized TiO<sub>2</sub> and the effect of adsorbates and light intensity on charge-carrier dynamics. *J. Chem. Soc., Faraday Trans.* **1994**, *90* (21), 3323–3330.
- (38) Schins, J. M.; Talgorn, E. Conductive response of a photo-excited sample in a radio-frequency driven resonance cavity. *Rev. Sci. Instrum.* **2011**, *82* (6), 064703.
- (39) Gao, Y.; Sandeep, C. S. S.; Schins, J. M.; Houtepen, A. J.; Siebbeles, L. D. A. Disorder strongly enhances Auger recombination in conductive quantum-dot solids. *Nat. Commun.* **2013**, *4*, 2329.
- (40) Savenije, T. J.; Huijser, A.; Vermeulen, M. J. W.; Katoh, R. Charge carrier dynamics in TiO<sub>2</sub> nanoparticles at various temperatures. *Chem. Phys. Lett.* **2008**, *461* (1), 93–96.
- (41) Marino, E.; Kodger, T. E.; Crisp, R. W.; Timmerman, D.; MacArthur, K. E.; Heggen, M.; Schall, P. Repairing Nanoparticle Surface Defects. *Angew. Chem.* **2017**, *129* (44), 13983–13987.
- (42) Bozyigit, D.; Lin, W. M. M.; Yazdani, N.; Yarema, O.; Wood, V. A quantitative model for charge carrier transport, trapping and recombination in nanocrystal-based solar cells. *Nat. Commun.* **2015**, *6*, 6180.
- (43) Talgorn, E.; de Vries, M. A.; Siebbeles, L. D. A.; Houtepen, A. J. Photoconductivity Enhancement in Multilayers of CdSe and CdTe Quantum Dots. *ACS Nano* **2011**, *5* (5), 3552–3558.
- (44) Grimaldi, G.; Crisp, R. W.; ten Brinck, S.; Zapata, F.; van Ouwendorp, M.; Renaud, N.; Kirkwood, N.; Evers, W. H.; Kinge, S.; Infante, I.; Siebbeles, L. D. A.; Houtepen, A. J. Hot-electron transfer in quantum-dot heterojunction films. *Nat. Commun.* **2018**, *9* (1), 2310.
- (45) Dicker, G.; de Haas, M. P.; Siebbeles, L. D. A. Signature of exciton annihilation in the photoconductance of regioregular poly(3-hexylthiophene). *Phys. Rev. B: Condens. Matter Mater. Phys.* **2005**, *71* (15), 155204.
- (46) Ferguson, A. J.; Kopidakis, N.; Shaheen, S. E.; Rumbles, G. Dark Carriers, Trapping, and Activation Control of Carrier Recombination in Neat P3HT and P3HT:PCBM Blends. *J. Phys. Chem. C* **2011**, *115* (46), 23134–23148.
- (47) Oh, S. J.; Straus, D. B.; Zhao, T.; Choi, J.-H.; Lee, S.-W.; Gaubling, E. A.; Murray, C. B.; Kagan, C. Engineering the Surface Chemistry of Lead Chalcogenide Nanocrystal Solids to Enhance Carrier Mobility and Lifetime in Optoelectronic Devices. *Chem. Commun.* **2017**, *53* (4), 728–731.
- (48) Crisp, R. W.; Kroupa, D. M.; Marshall, A. R.; Miller, E. M.; Zhang, J.; Beard, M. C.; Luther, J. M. Metal Halide Solid-State Surface Treatment for High Efficiency PbS and PbSe QD Solar Cells. *Sci. Rep.* **2015**, *5*, 9945.
- (49) Tessier, M. D.; De Nolf, K.; Dupont, D.; Sinnaeve, D.; De Roo, J.; Hens, Z. Aminophosphines: A Double Role in the Synthesis of Colloidal Indium Phosphide Quantum Dots. *J. Am. Chem. Soc.* **2016**, *138* (18), 5923–5929.
- (50) Grigel, V.; Dupont, D.; De Nolf, K.; Hens, Z.; Tessier, M. D. InAs Colloidal Quantum Dots Synthesis via Aminopnictogen Precursor Chemistry. *J. Am. Chem. Soc.* **2016**, *138* (41), 13485–13488.
- (51) Mundy, M. E.; Ung, D.; Lai, N. L.; Jahrman, E. P.; Seidler, G. T.; Cossairt, B. M. Aminophosphines as Versatile Precursors for the Synthesis of Metal Phosphide Nanocrystals. *Chem. Mater.* **2018**, *30*, 5373.
- (52) Yarema, M.; Caputo, R.; Kovalenko, M. V. Precision synthesis of colloidal inorganic nanocrystals using metal and metalloids amides. *Nanoscale* **2013**, *5* (18), 8398–8410.
- (53) Tessier, M. D.; Dupont, D.; De Nolf, K.; De Roo, J.; Hens, Z. Economic and Size-Tunable Synthesis of InP/ZnE (E = S, Se) Colloidal Quantum Dots. *Chem. Mater.* **2015**, *27* (13), 4893–4898.
- (54) Gur, I.; Fromer, N. A.; Geier, M. L.; Alivisatos, A. P. Air-Stable All-Inorganic Nanocrystal Solar Cells Processed from Solution. *Science* **2005**, *310* (5747), 462–465.
- (55) Panthani, M. G.; Kurley, J. M.; Crisp, R. W.; Dietz, T. C.; Ezzyat, T.; Luther, J. M.; Talapin, D. V. High Efficiency Solution Processed Sintered CdTe Nanocrystal Solar Cells: The Role of Interfaces. *Nano Lett.* **2014**, *14* (2), 670–675.
- (56) Kurley, J. M.; Panthani, M. G.; Crisp, R. W.; Nanayakkara, S. U.; Pach, G. F.; Reese, M. O.; Hudson, M. H.; Dolzhenkov, D. S.; Tanygin, V.; Luther, J. M.; Talapin, D. V. Transparent Ohmic Contacts for Solution-Processed, Ultrathin CdTe Solar Cells. *ACS Energy Letters* **2017**, *2* (1), 270–278.
- (57) Nag, A.; Kovalenko, M. V.; Lee, J.-S.; Liu, W.; Spokoyny, B.; Talapin, D. V. Metal-free Inorganic Ligands for Colloidal Nanocrystals: S<sup>2-</sup>, HS<sup>-</sup>, Se<sup>2-</sup>, HSe<sup>-</sup>, Te<sup>2-</sup>, HTe<sup>-</sup>, TeS<sub>3</sub><sup>2-</sup>, OH<sup>-</sup>, and NH<sub>2</sub><sup>-</sup> as Surface Ligands. *J. Am. Chem. Soc.* **2011**, *133* (27), 10612–10620.
- (58) Kovalenko, M. V.; Bodnarchuk, M. I.; Zaumseil, J.; Lee, J.-S.; Talapin, D. V. Expanding the Chemical Versatility of Colloidal Nanocrystals Capped with Molecular Metal Chalcogenide Ligands. *J. Am. Chem. Soc.* **2010**, *132* (29), 10085–10092.
- (59) Reid, O. G.; Moore, D. T.; Li, Z.; Zhao, D.; Yan, Y.; Zhu, K.; Rumbles, G. Quantitative analysis of time-resolved microwave conductivity data. *J. Phys. D: Appl. Phys.* **2017**, *50* (49), 493002.
- (60) Kim, M. S.; Yim, K. G.; Kim, S.; Nam, G.; Lee, D. Y.; Kim, J. S.; Kim, J. S.; Leem, J. Y. Growth and Characterization of Indium-Doped Zinc Oxide Thin Films Prepared by Sol-Gel Method. *Acta Phys. Pol., A* **2012**, *121* (1), 217–220.
- (61) Ohyama, M.; Kozuka, H.; Yoko, T. Sol-gel preparation of transparent and conductive aluminum-doped zinc oxide films with highly preferential crystal orientation. *J. Am. Ceram. Soc.* **1998**, *81* (6), 1622–1632.